JACS
JOURNAL OF THE AMERICAN CHEMICAL SOCIETY
Article
pubs.acs.org/JACS

# The Nature of Singlet Exciton Fission in Carotenoid Aggregates

Andrew J. Musser,*[,†] Margherita Maiuri,[‡] Daniele Brida,[§] Giulio Cerullo,[‡] Richard H. Friend,[†] and Jenny Clark[∥]

[†]Cavendish Laboratory, University of Cambridge, Cambridge CB3 0HE, United Kingdom
[‡]IFN-CNR, Dipartimento di Fisica, Politecnico di Milano, I-20133 Milano, Italy
[§]Department of Physics and Center for Applied Photonics, University of Konstanz, D-78457 Konstanz, Germany
[∥]Department of Physics and Astronomy, University of Sheffield, Sheffield S3 7RH, United Kingdom

Supporting Information

**ABSTRACT:** Singlet exciton fission allows the fast and efficient generation of two spin triplet states from one photoexcited singlet. It has the potential to improve organic photovoltaics, enabling efficient coupling to the blue to ultraviolet region of the solar spectrum to capture the energy generally lost as waste heat. However, many questions remain about the underlying fission mechanism. The relation between intermolecular geometry and singlet fission rate and yield is poorly understood and remains one of the most significant barriers to the design of new singlet fission sensitizers. Here we explore the structure−property relationship and examine the mechanism of singlet fission in aggregates of astaxanthin, a small polyene. We isolate five distinct supramolecular structures of astaxanthin generated through self-assembly in solution. Each is capable of undergoing intermolecular singlet fission, with rates of triplet generation and annihilation that can be correlated with intermolecular coupling strength. In contrast with the conventional model of singlet fission in linear molecules, we demonstrate that no intermediate states are involved in the triplet formation: instead, singlet fission occurs directly from the initial $1B_u$ photoexcited state on ultrafast time scales. This result demands a re-evaluation of current theories of polyene photophysics and highlights the robustness of carotenoid singlet fission.

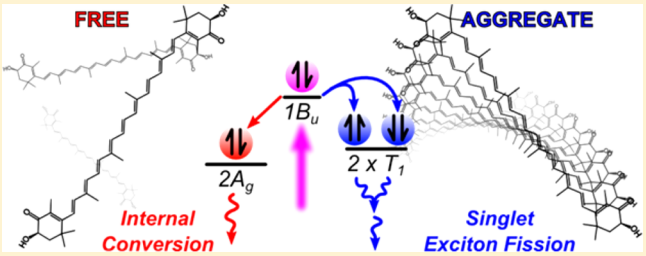


## INTRODUCTION

Singlet exciton fission is the quantum mechanical process by which a singlet exciton splits into two distinct spin triplet excitons. The triplets are initially coupled into an overall singlet state, conserving spin and allowing for extremely fast and highly efficient triplet formation.[1−3] This phenomenon has recently become the object of intense study due to its proposed use for carrier multiplication in solar cells.[4] Singlet fission has already been successfully harnessed in devices,[5−9] in some exceptional cases with an internal quantum efficiency near 200%.[10,11] The record external quantum efficiency in these systems of 135% is the highest achieved for any photovoltaic technology, demonstrating the great potential of singlet fission devices. Further practical advances will demand a more thorough understanding of the underlying mechanism of singlet fission, as well as how it relates to intermolecular structure. For example, it has been shown in amorphous films of diphenyltetracene that long-range order is not required for efficient triplet formation,[12] but other studies on disordered systems highlight the importance of specific local interactions.[13,14] These local interactions, and particularly the strength of intermolecular coupling, have been proposed to play a central role in determining the rate and dominant mechanism of singlet fission—nonadiabatic or adiabatic—in a new model covering all acenes.[15]

This significant progress has occurred almost exclusively within a relatively narrow class of materials: tetracene, pentacene, and their derivatives. This restricts the understanding of structure−property relationships and singlet fission mechanisms needed to develop new materials and broaden the library of candidate chromophores. One class of materials with significant promise for singlet fission is the polyenes,[1] which are characterized by a low-lying (dark) excited state of the same $A_g$ symmetry as the ground state. The theoretical basis for fission in these materials lies in the symmetry of this state, which has an equivalent description as a weakly coupled pair of triplet excitons, suggesting the possibility of intramolecular singlet fission.[16] Indeed, intramolecular singlet fission has been observed in some conjugated polymers.[17−21] However, as we have previously shown in poly(3-dodecylthienylenevinylene), intramolecular singlet fission does not actually proceed via the expected $2A_g$ state but occurs directly from the initially photoexcited $1B_u$ exciton.[21] In carotenoids, too, singlet fission has been observed; these polyenes are evidently too short to support intramolecular triplet pair formation but undergo singlet fission in biological complexes with proteins[22−24] or in self-assembled aggregates.[25−27] It is not clear how the original

Received: February 4, 2015
Published: March 31, 2015




DOI: 10.1021/jacs.5b01130
J. Am. Chem. Soc. 2015, 137, 5130−5139

$2A_g$ mediated mechanism can be extended to these materials, as the model is fundamentally intramolecular in nature. Wang and Tauber[25] have suggested that singlet fission in carotenoid aggregates does not involve the $2A_g$ state, but no studies have been made with sufficient time resolution to confirm this hypothesis.

Here we use broadband transient absorption spectroscopy from the tens of femtoseconds to microseconds time scales to investigate the singlet fission process in aggregates of the carotenoid astaxanthin (Figure 1a). We study a series of five distinct aggregates to determine both the role of intermolecular structure and the interplay between triplet formation and internal conversion to the $2A_g$ state. We show that intermolecular singlet fission in polyenes follows the same mechanism—direct formation from $1B_u$ (Figure 1d)—observed in the intramolecular polymer system reported previously.[21] The initial rate of triplet formation is seen to only weakly correlate with the strength of intermolecular coupling with a fastest time constant of only 65 fs, among the fastest of any reported system. These results raise important questions about the electronic structure and intermolecular interactions of the polyenes and also point the way toward a universal mechanism for ultrafast singlet fission.

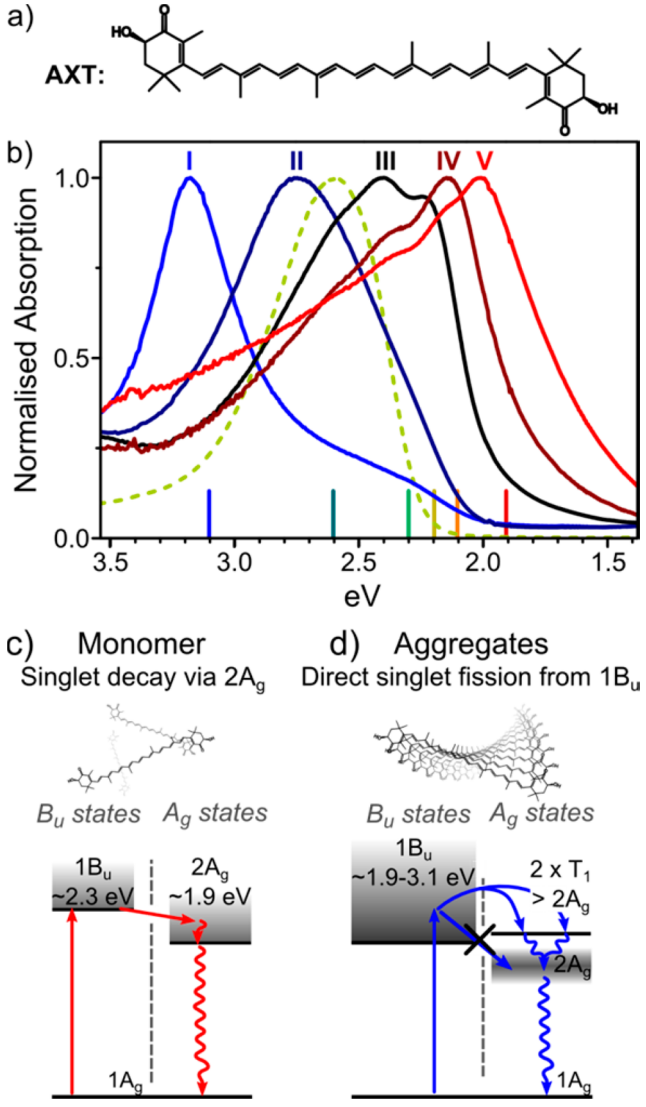


**Figure 1.** Aggregation of astaxanthin. (a) AXT chemical structure. (b) Normalized UV−vis absorption of five stable aggregates of AXT in 9:1 water:DMSO (I and II) or 4:1 water:acetone (III−V) as well as monomeric AXT in acetone (dashed). Vertical lines indicate pump photon energies used for TA measurements. (c) Model of exciton decay in monomeric AXT. Ultrafast internal conversion from $1B_u$ to $2A_g$ is followed by fast nonradiative decay to the ground state. (d) Model of singlet fission and triplet annihilation in carotenoid aggregates, as measured here. Upon aggregation, the $1B_u$ state no longer couples to $2A_g$. Instead, it converts directly into triplet pairs via singlet fission. The $2A_g$ state is lower in energy than the triplet pair and enables efficient recombination back to the ground state.

## EXPERIMENTAL SECTION

Racemic astaxanthin (AXT) was generously donated by BASF. Type-A gelatin and $C_{60}$ fullerene were purchased from Sigma-Aldrich. Enantiomerically pure 3*S*,3′*S*-, 3*S*,3′*R*-, and 3*R*,3′*R*-astaxanthin for circular dichroism measurements were purchased from CaroteNature. All materials were used as received without further purification.

AXT monomer solutions were prepared at a concentration of 100 $\mu$M in acetone or DMSO and heated at 50 °C until clear. The series of five distinct, stable aggregate solutions (Figure 1a) was prepared as follows. For aggregate I a 420 $\mu$M solution of AXT in DMSO at room temperature was mixed in a 1:9 ratio with water at 5 °C. Aggregate II was prepared by mixing a 1000 $\mu$M solution of AXT in DMSO at 80 °C in a 1:9 ratio with water at 80 °C. The three red-shifted aggregates were prepared instead from acetone stock solutions heated to 65 °C, and to impart long-term colloidal stability, type-A gelatin aqueous solutions at 50 °C were used instead of pure water.[28,29] The organic:aqueous mixing ratio for all three species was 1:4. Aggregate III used an AXT concentration of 250 $\mu$M and a 5 mg/mL gelatin solution. The AXT stock concentration for aggregate IV was 375 $\mu$M, with a gelatin concentration of 2.5 mg/mL. Aggregate V was prepared with the same acetone stock as aggregate IV and a higher gelatin content of 10 mg/mL, and the solution was heated at 65 °C for an additional 10 min after mixing. All aggregate solutions were stored in the dark at room temperature. Time-resolved measurements were only performed on aggregates that were stable for >1 week.

Sub-picosecond transient absorption (TA) measurements were performed on a previously reported setup[21] with slight modifications. Narrow-band (~10 nm) excitation pulses were generated in an optical parametric amplifier (TOPAS, Light Conversion Ltd.) coupled to the output of a 1 kHz regenerative amplifier (Spectra-Physics Solstice). To ensure that TA spectra reflected specific aggregate types rather than mixtures of species, pump photon energies were scanned across the aggregate absorption bands (vertical lines in Figure 1a), with typical pump fluences below $4 \times 10^{14}$ photons/pulse-cm$^2$. Because excessive pump fluence results in spurious ultrafast effects, all measurements were also performed at lower fluence, and the fluence dependence was studied in detail for all samples (see below). The sample transmission was probed using broadband pulses generated in two home-built non-collinear optical parametric amplifiers (NOPAs) roughly spanning 0.75−2.5 eV.[30,31] The probe beam was split to provide a reference signal not affected by the pump to mitigate any laser fluctuation effects, and both were dispersed in a spectrometer (Andor, Shamrock SR-303i) and detected using a pair of linear image sensors (Hamamatsu, G11608) driven and read out at the full laser repetition rate by a custom-built board from Stresing Entwicklungsbüro. The differential transmission ($\Delta T/T$) was then measured as a function of probe photon energy and pump−probe delay. This setup afforded a temporal resolution of approximately 120 fs. The same setup was employed for nanosecond TA, using the frequency-doubled (2.33 eV) nanosecond output of a Q-switched Nd:YVO4 laser as the excitation source. High-time-resolution measurements were also performed on a similar setup, in which both the pump and probe beams were generated by home-built NOPAs generating sub-30 fs (pump) and sub-10 fs (probe) pulses using chirped mirror compression.


DOI: 10.1021/jacs.5b01130
J. Am. Chem. Soc. 2015, 137, 5130−5139

## RESULTS AND DISCUSSION

The spectra in Figure 1a demonstrate the great potential of astaxanthin (AXT) aggregates for a study of structure−property relations in singlet fission. This system is noteworthy both for the large number of distinct aggregates formed and the wide range over which the primary absorption band can be tuned—approximately 1.2 eV—through simple control of water content, temperature, and gelatin stabilization. AXT also appears to be unique in having two blue-shifted structures and the strongly red-shifted aggregate V, which is unlike any other reported carotenoid aggregates.

We consider that the UV−vis absorption spectra shown here represent distinct aggregate types, rather than mixed populations. Because these aggregates form through gradual transitions from one species to the next (see Supporting Information, Figures S1 and S2), it is easy to generate mixtures of species through slight changes in preparation conditions. In all cases, the UV−vis spectra of such samples can be decomposed into the species shown in Figure 1a. To control for the possibility of aggregate mixtures, we performed TA measurements with selective excitation across the absorption band (see below and Supporting Information, Figures S6−S10). Only aggregate III showed an excitation dependence suggestive of heterogeneity.

The determination of the structure of carotenoid aggregates is a long-standing problem,[32−37] and the diversity of intermolecular packing attained here highlights its complexity. From the UV−vis absorption spectra alone, little can be determined about the relevant intermolecular parameters. In the absence of vibronic structure at room temperature,[38] we cannot quantify changes in the 0 0/0−1 peak ratios. Likewise, the degree of red- or blue-shift, a gauge of the strength of exciton coupling, cannot be determined precisely due to significant solvatochromism (see Supporting Information, Figure S3). We focus instead on a qualitative description. Aggregate I is strongly blue-shifted and exhibits significant narrowing of the absorption band—it is best described as a strongly coupled H-aggregate. Aggregate II exhibits a weaker blue-shift as well as a change in shape that would be consistent with a decrease in the 0−0/0−1 peak ratio, making it most likely a weakly coupled H-aggregate. Aggregate III is a borderline case which would typically be described as a J-aggregate, but on the basis of Spano's analysis of lutein aggregates,[37] it may equally be a very weakly coupled H aggregate. The appearance of a pronounced 0−0 peak and strong red-shift in aggregates IV and V is characteristic of J-aggregation, which is presumed to be the primary interaction in these species.

Further insight can be gained from comparison to reported spectra. Aggregates similar to I are almost exclusively formed by carotenoids with at least one hydroxyl group on the terminal rings, pointing to the importance of intermolecular hydrogen bonding.[33,39] The observed sensitivity of the formation of I to pH is consistent with this motif. Furthermore, the absorption spectrum of crustochrin, a carotenoprotein predominant in yellow lobster carapace, is almost identical to that of aggregate I, and the two share similar Raman signatures.[40] However, that protein has never been crystallized, and little is known about the orientation or coupling of the AXT molecules in this material. Aggregates such as II are preferentially formed by carotenoids with carbonyl but no hydroxyl groups;[33] it is likely that in this species the supramolecular structure is primarily mediated through the C−H···O motif described by Bartalucci et al.[41] for crystals of AXT and canthaxanthin. Strongly red-shifted AXT aggregates such as IV and V have long been studied in the context of lobster coloration. The primary carotenoprotein in lobster carapace, crustacyanin, exhibits a similarly pronounced red shift.[41−43] Recent studies attribute the bulk of this effect to planarization of the AXT molecules within the protein so that the terminal rings lie in trans conformation, with a consequent extension of the conjugation length.[42] Indeed, the spectra of IV and V each closely match different portions of the reported absorption of a crystal of an all-trans AXT derivative.[43] We thus consider species IV and V to contain all-trans AXT, with packing similar to the reported crystal structure. The fact that each aggregate agrees so well with a separate section of the crystal spectrum indicates the presence of two polymorphs in the solid state.

The UV−vis absorption and circular dichroism data (Supporting Information, Figure S4) at hand are insufficient to reliably determine the intermolecular packing in these aggregates, and further structural characterization is needed. For our purposes here, it is sufficient to rank them by approximate strength of intermolecular coupling: I > V > IV > III ∼ II.

**Monomeric AXT Photophysics.** To establish a baseline for the photophysical behavior of AXT, we first examine the excited state processes of monomeric AXT in pure organic solution. Because the carotenoids exhibit pronounced solvatochromism (Suporting Information, Figure S3), monomer solutions were prepared in both acetone and DMSO. The key results of TA measurements on AXT monomers excited at the absorption maximum are presented in Figure 2. Our TA results are presented throughout in units of $\Delta T/T$, in which the absorption of photogenerated states appears negative. Positive features can reflect either increased transmission of the probe through the sample due to bleaching of the ground state or probe amplification arising from stimulated emission. Using 120 fs excitation pulses, the results for the two solvents were almost identical save for a slight red-shift of all photoinduced absorption (PIA) features in DMSO (Figure S3), so only the acetone data will be addressed here. AXT shows the characteristic polyene behavior illustrated in Figure 1c and can be described in terms of just two states.

Within the instrument response (black trace), a sharp PIA can be detected between 1.0 and 1.5 eV, accompanied by a positive feature around 2.25 eV which agrees well with steady-state photoluminescence spectra and can be assigned to stimulated emission. These are the signatures of the initial $1B_u$ exciton, which decays with instrument-limited kinetics to the dark $2A_g$ state (green traces). This state shows a pronounced PIA peaked at 2.05 eV as well as a weak PIA tail at the low-energy edge of the available spectral range, assigned to the $2A_g \rightarrow 1B_u$ transition.[44] As in other polyenes, after fast thermalization the $2A_g$ state decays uniformly and non-radiatively back to the ground state through efficient coupling to the vibrational manifold. We thus treat the monomer decay as following the simple model of $1B_u \rightarrow$ hot $2A_g \rightarrow 2A_g \rightarrow 1A_g$ (ground state).

The entire spectral range can be fitted well with three time constants: an instrument-limited 120 fs constant describing the internal conversion from $1B_u$, a 200 fs thermalization within the $2A_g$ manifold and a 5 ps final decay to the ground state. This behavior is completely independent of pump fluence for all spectral features over nearly 2 orders of magnitude (Figure 2b).


DOI: 10.1021/jacs.5b01130
J. Am. Chem. Soc. 2015, 137, 5130−5139

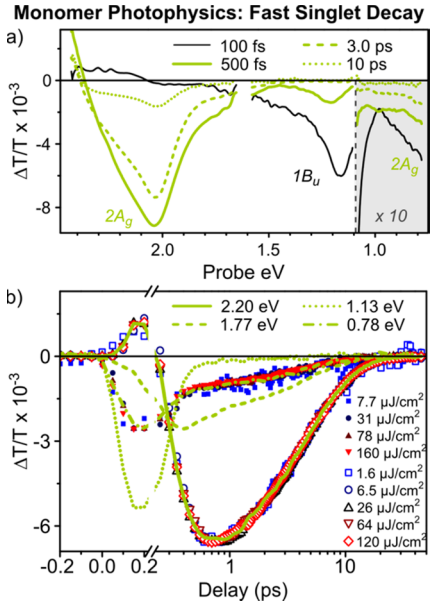


**Figure 2.** Monomer transient absorption. (a) Selected sub-ps TA timeslices following excitation at 2.6 eV with 26 $\mu$J/cm$^2$. A three-state model is sufficient to describe these data. The initial $1B_u$ PIA can only be clearly observed within the pump pulse duration (black), and it decays to form the well-known $2A_g$ PIA in the visible region. The region below 1.1 eV is magnified 10× to show the weak $2A_g \rightarrow 1B_u$ PIA. (b) The corresponding decay kinetics (lines) show direct, instrument-limited conversion from $1B_u$ to $2A_g$ and rapid decay to the ground state. These processes are completely independent of pump fluence over nearly 2 orders of magnitude (symbols, data normalized with respect to pump intensity) The data for 0.78 eV are magnified by a factor of 4 for clarity.

There is no sign of or apparent need for intermediate states between $1B_u$ and $2A_g$ to explain these results, as confirmed with sub-30 fs TA measurements (see below). It should be stressed that there is also no sign of triplet formation by singlet fission or any other process at any pump photon energy; individual carotenoid molecules are evidently too small to support triplet pair states.

**Carotenoid Aggregate Photophysics.** TA measurements were performed on all five aggregates at four or more pump photon energies. Due to the overall similarity of the aggregate TA data, only the representative aggregates II (weak H-aggregate) and IV (strong J-aggregate) will be discussed in detail here. The spectra of other aggregates and other pump photon energies can be found in the Supporting Information, Figures S5−S10. Comparison of the TA spectra for aggregate II in Figure 3a,b with the monomer data in Figure 2 reveals two immediate differences: the PIA bands are broader and much less pronounced in II, and the final decay is significantly slower. As will be shown below in Figure 4, the final state in this aggregate is the triplet. Its PIA is dominant well before 3 ps (see below), and the spectrum decays without further evolution out to the $\mu$s time scale. The only spectral changes that can be clearly discerned occur on an ultrafast instrument-limited time scale: much like in monomeric AXT the initial excited state absorbs in the NIR, seen as a broad, weak PIA in the earliest TA spectrum. As shown in Figure 3c, the decay of the NIR band is matched by the decay of the slight ground-state bleach (GSB) observed around 2.4 eV. This kinetic reflects the sub-ps formation of triplet PIA, which strongly overlaps with the ground-state absorption and results in a negative overall signal.

On first inspection the TA results for IV in Figure 3d−f appear quite different from those obtained for aggregate II.

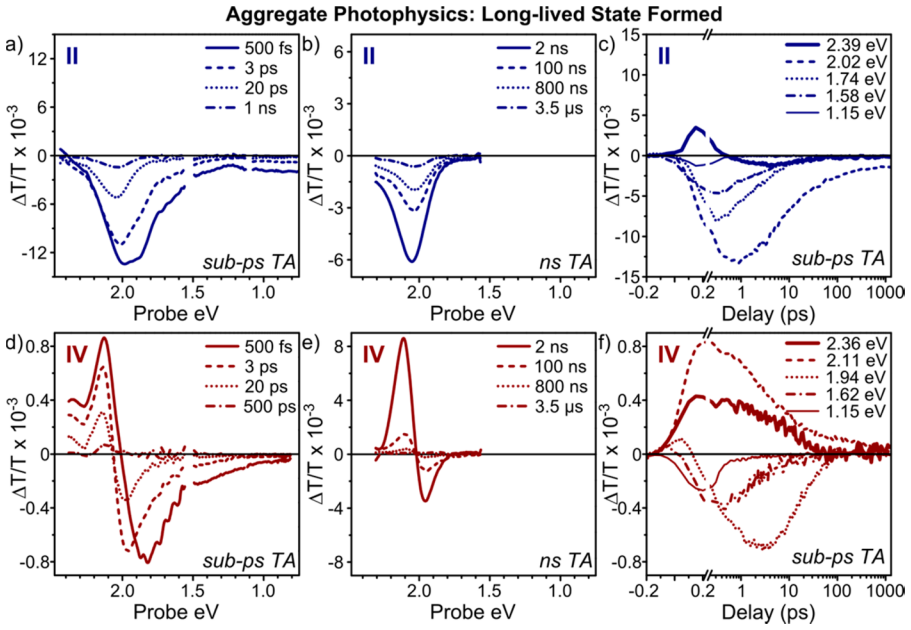


**Figure 3.** Transient absorption of AXT aggregates. (a) Selected timeslices from sub-ps TA of II excited at 2.6 eV. The prompt decay of the broad NIR PIA is the only significant spectral change in the entire measurement range and reflects internal conversion from the initial $1B_u$ state. (b) Timeslices from ns TA show continued uniform decay of the state formed within 3 ps. (c) Integrated decay kinetics from sub-ps TA reveal instrument-limited decay of the GSB and NIR PIA (solid lines) to form the final state. (d) Equivalent sub-ps measurement of IV excited at 2.3 eV, showing similar rapid decay of the initial band in the NIR and formation of the final state within 3 ps, which (e) uniformly decays on the $\mu$s time scale. (f) Integrated decay kinetics from sub-ps TA of IV show an instrument-limited internal conversion from the initial state (thin solid line) similar to II. The slower rise at 1.94 eV reflects a gradual shift of the crossing point between GSB and PIA, related to the generation of vibrationally excited ground states following nonradiative decay of triplet pairs.[21]



DOI: 10.1021/jacs.5b01130
J. Am. Chem. Soc. 2015, 137, 5130−5139

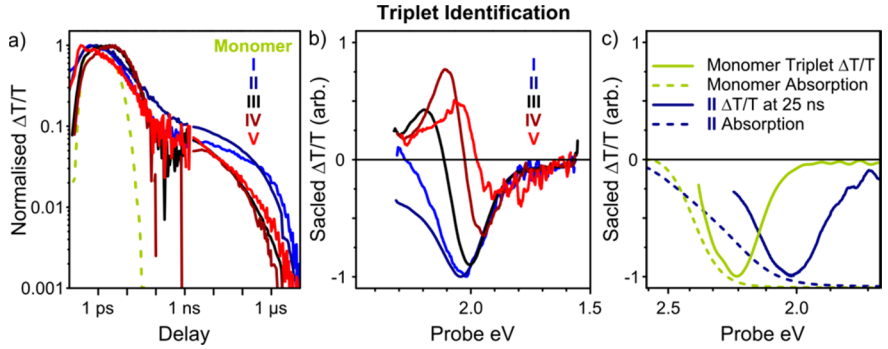


**Figure 4.** Triplet identification. (a) Integrated decay kinetics from all species, at the peak of PIA, following excitation at 2.3 eV. All aggregates (solid) show an enhancement of the final state lifetime of 5 orders of magnitude, relative to the monomer (dashed). (b) Comparison of the TA signal at 100 ns for all five aggregates reveals the same PIA signature in each, combined with a GSB related to the UV−vis absorption. The final state must be the same in all aggregates. (c) Comparison of the absorption edge (dashed) and long-lived TA signal (solid) of monomer AXT following triplet sensitization (green) and aggregate II. The similarity of shape confirms the assignment of the long-lived aggregate state to triplets, produced via singlet fission.

However, they reflect essentially the same photophysics. The most prominent difference is the sharp positive $\Delta T/T$ band above 2.0 eV. This signal perfectly matches the position of the vibronic peaks observed in steady-state absorption (Figure 1a) and can be assigned to GSB of the aggregate. As in Figure 3a, an ultrafast decay from the initial $1B_u$ state can be inferred from the instrument-limited loss of the PIA in the NIR along with a matching rise of PIA in the visible and a slight blue-shift of the GSB edge. The final state in this aggregate—again formed on ultrafast time scales—is the same as in aggregate II, namely triplet excitons.

Indeed, all five aggregates form triplets on ultrafast time scales, with most spectral evolution complete by 1 ps. In a system such as aggregated AXT, with no heavy atoms and no significant intersystem crossing yield in free solution, the only mechanism for such fast triplet formation is singlet fission. We detect none of the signatures of $2A_g$, such as $2A_g \rightarrow 1B_u$ PIA below 1 eV, or of any other excited state within the ∼120 fs temporal resolution of this measurement. We thus propose that intermolecular singlet fission in this polyene system occurs directly from the $1B_u$ exciton, the same mechanism we observed for intramolecular singlet fission in poly(3-thienylenevinylene).[21] This claim is confirmed below with sub-30 fs TA.

Figure 4 compares the final state observed in each aggregate following excitation at 2.33 eV. We first highlight the dramatic enhancement of the final state lifetime upon aggregation, by roughly 5 orders of magnitude. Only thermal effects[45] or the formation of charged species or triplet excitons would be expected to yield such long lifetimes. The only long-lived features are found in the visible spectral region (Figure 4b). The agreement of the PIA bands on the low-energy side of the spectrum is striking, and the differences at higher energies can be accounted for as different GSB contributions, related to the shape of the ground-state absorption spectra. This comparison not only confirms that the same long-lived species is present in every sample but also ensures that it is an excited state of the primary aggregate type observed in UV−vis absorption rather than a minority population. The close spectral overlap of the PIA bands allows us to rule out pump-induced thermal modulation, as it is highly unlikely for this effect to produce the same red-absorbing species in five widely varied aggregate structures with absorption edges varying by ∼1.5 eV. We can also rule out charge formation, as the characteristic NIR absorption bands of carotenoid anions and cations are absent in all cases.[46−49]

These considerations already enable an assignment of the terminal long-lived state to triplet excitons, and for further confirmation we use the triplet sensitization technique of Sasaki et al.[50] Briefly, a mixed solution of AXT and $C_{60}$ in toluene was excited at 2.33 eV with the long-delay TA setup. Within the pump pulse duration, we observe the decay of AXT singlets and formation of triplet excitons on $C_{60}$ (Supporting Information, Figure S11). On a hundreds of picoseconds time scale, the triplet excitons undergo triplet energy transfer to AXT, resulting in the sharp characteristic PIA of carotenoid triplets (Figures 4c, green, and S11). Comparison with our long-delay spectra, using only aggregate II for clarity, shows a similar overall shape. However, the long-lived signal in aggregates is slightly broader and red-shifted by ∼0.2 eV. A small red-shift for carotenoid triplet absorption in aggregates or complexes has been previously observed[39,51] and can be partially attributed to the change in dielectric environment upon aggregation. Moreover, the shift is comparable to that observed in the ground state absorption edge (dashed lines), which may indicate that GSB also contributes to the apparent red shift.

As for the spectral broadening, it is actually a consequence of singlet fission. The same phenomenon has been observed in poly(3-dodecylthienylenevinylene)[21] and in polydiacetylene.[18] In the latter work it was proposed that the initial geminate triplet pairs still interact following singlet fission, though they are no longer fully coupled into a singlet state. These interactions perturb the triplet energy levels, leading to a broadening and further red-shift of the PIA. The agreement of our results with a similar system[25,26] and the reasonable match between the long-lived spectrum and the triplet reference are sufficient to conclude that the final state in all AXT aggregates is triplet excitons.

The match of this triplet PIA across the entire aggregate series is striking and merits further consideration. We recall that optically allowed transition varies by ∼1 eV between aggregates I and V, demonstrating the strong effect of aggregation on the singlet excited state. On the other hand, the most significant effect on the $T_1 \rightarrow T_n$ absorption band in Figure 4 is the mere fact of aggregation: all aggregates share approximately the same redshift of this band relative to the sensitized monomer triplet. This result is a likely consequence of the highly localized nature of carotenoid triplets. Whereas the precise nature of the


DOI: 10.1021/jacs.5b01130
J. Am. Chem. Soc. 2015, 137, 5130−5139

nearest-neighbor coupling within the aggregates can strongly influence singlet absorption, the triplet only reflects bulk-type dielectric effects. On the basis of this behavior, we can be confident that the energy of the triplet exciton does not change through aggregation.

**Triplet Decay.** Though all of the aggregates undergo the same process of singlet fission, the kinetics in Figure 4a reveal clear differences in the subsequent fate of the triplets. To better understand this behavior, we begin by evaluating the dependence of these kinetics on pump fluence in detail for aggregate II (see Supporting Information, Figures S13 and S14 for qualitatively similar results for the other aggregates).

We first consider the ps-ns regime (Figure 5a), during which the triplet PIA spectrum decays uniformly with at most a slight narrowing (Figure 3a). The multiexponential decay we observe on these time scales is far too short for the intrinsic triplet lifetime. Instead, in agreement with studies of zeaxanthin aggregates[26,39] we attribute this behavior to annihilation processes, specifically triplet−triplet annihilation (TTA). This is a highly efficient process—though some fraction of the triplets survives out to $\mu$s time scales, at least 90% of the excited population annihilates between 1 ps and 1 ns. At the same time, this initial TTA regime is completely independent of pump fluence and must thus correspond to the annihilation of geminate triplet pairs. These facts enable an important insight into the energetics of singlet fission in carotenoids.

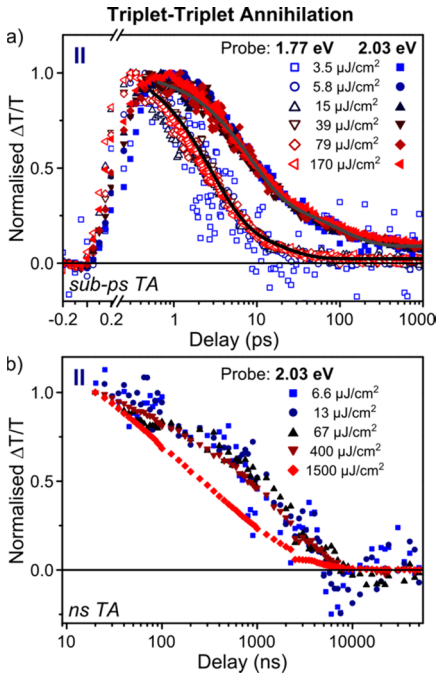


**Figure 5.** Regimes of triplet−triplet annihilation in aggregate II. (a) Integrated decay kinetics of II following sub-ps excitation at 2.6 eV. The same multiexponential function fits the decay at all fluences, requiring the recombination process to be entirely geminate. Lifetimes (0.9, 6, and 49 ps) are not assigned to individual processes but rather reflect the wide distribution of triplet pair decay rates. (b) Integrated decay kinetics of II on longer time scales, following ns excitation at 2.3 eV, show strong fluence dependence indicative of non-geminate TTA.

According to the conventional energy scheme $1B_u > 2A_g > 2T_1 > T_2$, only one pathway for TTA is permitted: $T_1 + T_1 \rightarrow T_2 + S_0 \rightarrow T_1 + S_0$. Such a model could potentially explain a prompt loss of 50% of the triplet population through geminate TTA, but any further losses would depend on intrinsically slow triplet diffusion. This latter process would be strongly dependent on excitation density, which cannot be reconciled with the fast, fluence-independent decay observed here. A further consideration is the very nature of triplets produced through singlet fission. The usual treatment of TTA assumes a randomized population of triplets, such that pairs of triplets can couple and annihilate into an overall spin singlet or spin triplet state. However, the initial triplet population here is anything but random. The triplet pair produced through fission is by definition coupled into a spin singlet, so TTA is only possible back to a singlet state until the coherence is broken by spin−lattice relaxation, which occurs on longer time scales. Thus, fast geminate recombination of the type $T_1 + T_1 \rightarrow T_2 + S_0$ should not be possible, even if it is energetically favorable.

Instead, the only available pathway for geminate TTA that passes through another electronic state is $T_1 + T_1 \rightarrow S_1$ (i.e., $2A_g$) + $S_0$. This process would be completely independent of excitation density and could proceed on a range of time scales, governed by the couplings in the distribution of triplet pair states formed. In short, this model of TTA very closely matches the results presented in Figures 5a and S13 on AXT aggregates. This requires a reevaluation of the standard energetic scheme in carotenoids. It is generally accepted that $1B_u > 2A_g > 2T_1 > T_2$, with a relatively small gap between $2A_g$ and $2T_1$. However, triplet energies are notoriously difficult to measure, particularly in the absence of phosphorescence, and if the $T_1$ energy were even slightly higher, the state ordering would become $1B_u > 2T_1 > 2A_g$.

On the longer time scales shown in Figure 5b, the relatively few triplets that survive the initial TTA regime are stabilized and do not appear to undergo geminate recombination. Instead, they are free to diffuse and decay with a strong fluence dependence, a clear indicator of non-geminate TTA. At lower fluences the final decay still converges well to a single exponential decay of ~1.25 $\mu$s, which is reasonable as the intrinsic triplet lifetime, but at the highest excitation density the triplet decay is distinctly nonexponential over the entire range. It is important to note here that the fluence behavior is more complicated than in standard bimolecular recombination, as the ability of the triplets to annihilate depends not only on the rate of triplet diffusion but also on the distribution of aggregate sizes, both quantities unknown but likely to vary across the aggregate series.

With this understanding of TTA in AXT aggregates, we return to the kinetics in Figure 4a. The fastest initial decay is observed for the aggregates I and V that exhibit the strongest intermolecular coupling—as would be anticipated, the triplet pairs formed by singlet fission are similarly more strongly coupled and annihilate quickly.[1] Conversely, the decay over the first 1 ns is slowest in the relatively weakly coupled aggregate II. The dependence on excitation density and strong variation in absorption cross-section between aggregates preclude direct comparison of the longer-time decay kinetics, though all exhibit a similar characteristic lifetime of order 1 $\mu$s.

**Ultrafast Triplet Formation.** As noted above, the process of singlet fission identified in Figure 3 is largely complete within the instrument response of the sub-ps TA experiment. To fully resolve the triplet formation, we performed sub-30 fs TA measurements on the full set of aggregates as well as monomeric AXT in acetone and DMSO. In dilute solution (Figure 6) we find that the monomer reproduces the behavior observed previously using sub-ps TA, namely direct conversion


DOI: 10.1021/jacs.5b01130
J. Am. Chem. Soc. 2015, 137, 5130−5139

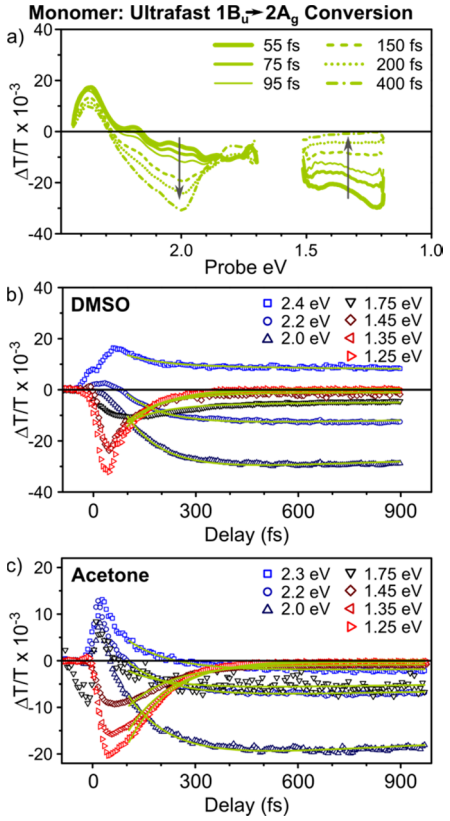


**Figure 6.** Ultrafast $1B_u \rightarrow 2A_g$ internal conversion. (a) Transient absorption timeslices from sub-30 fs TA on monomeric AXT in DMSO, showing smooth transition from $1B_u$ (PIA below 1.5 eV) to $2A_g$ (PIA above 1.8 eV). No other electronic state can be identified. Arrows indicate direction of spectral change. The corresponding decay kinetics (symbols) in (b) DMSO and (c) acetone can be well described with an exponential time constant (lines) of 105 or 125 fs, respectively.

of $1B_u$ into a hot $2A_g$ state which rapidly cools. The higher time resolution enables a clean determination of the $1B_u \rightarrow 2A_g$ internal conversion time constant, which we find to vary with solvent from 105 fs in DMSO to 125 fs in acetone with no discernible intermediate states. It is unclear what environment is most appropriate for comparison to AXT molecules embedded in (or at the surface of) aggregates, but this measurement establishes an approximate 100 fs time scale with which singlet fission must compete to proceed efficiently.

The results for aggregates II–IV, for which the fission process can be most clearly distinguished, are presented in Figure 7. Data for aggregates I and V can be found in the Supporting Information. In all cases, the spectra agree well with the sub-ps TA measurements on the same aggregates. The initial state in all species has a PIA in the NIR, in the same region where the $1B_u$ state absorbs in monomeric AXT. This band rapidly decays, resulting in the same triplet signature identified in Figure 4b. To capture the time scale of this process, the decay kinetics for each aggregate were globally fitted with a simple biexponential function, revealing two distinct temporal regimes: a sub-100 fs process that describes the formation of triplet PIA, and a slower (hundreds of femtoseconds) redshift consistent with thermalization of the hot triplet pair state. These fits give a singlet fission time constant of 85, 90, and 65 fs in aggregates II, III, and IV, respectively, distinctly faster than the ultrafast $1B_u \rightarrow 2A_g$ internal conversion detected in the monomer.

To confirm the assignments from these decay kinetics, the data were analyzed with a spectral decomposition technique based on a genetic algorithm.[52] In aggregates II–IV, the transition was best modeled with only two species (Figure 7d–f) showing the characteristic features of $1B_u$ and the triplet described above. We observe singlet fission directly from $1B_u$ on time scales consistent with the raw kinetic fitting and find no evidence of any other excited states.

The rates of triplet formation here are among the fastest reported for any intermolecular singlet fission system. This rapid fission cannot be explained solely by the energetic difference between singlet and triplet pair states: the triplet energy should not change with aggregation, while the singlet varies by over 1.2 eV. Using typical values,[26] we may even expect the singlet and triplet pair states to be nearly degenerate in aggregate V. The two weakly coupled aggregates II and III are the slowest, forming triplets with roughly the same time constant ~90 fs. Aggregate IV exhibits even faster singlet fission, which we propose is related to its stronger intermolecular coupling. Indeed, in the two most strongly coupled aggregates I and V we are unable to distinguish any state prior to triplets within the temporal resolution of the measurement, which was restricted in those systems to ~70 fs due to scattering and a strong coherent solvent response.

Unlike the initial rate of TTA, we find the rate of triplet formation is only weakly dependent on the strength of intermolecular coupling. Indeed, the mechanism of singlet fission in these aggregates must be remarkably robust: variation of the band gap over a range of 1.2 eV, with concomitant changes in the energetic driving force for triplet pair formation, yields fission time constants that span the narrow range ~50–100 fs. Even in the most weakly bound aggregates II and III, where singlet fission is only slightly faster than the expected $1B_u \rightarrow 2A_g$ time scale, we detect no signs of any other excited states, and we thus consider that this initial step is highly efficient in all aggregates.

The surprising result that the ultrafast $1B_u \rightarrow 2A_g$ internal conversion channel of the monomer is completely deactivated within the aggregates merits closer consideration. We note that this internal conversion is generally accepted to proceed via a conical intersection and is thus driven by nuclear motion.[53] It is conceivable that the same crossing is approached in the aggregates, with the important distinction that the strong exciton coupling ensures a delocalized state. The predicted triplet pair character of $2A_g$ results in a short-lived singlet state when it is confined to a single polyene chain, but delocalization over multiple chromophores may allow sufficient separation between the constituent triplets to give the state more triplet-like character. While such a model could explain the early time transient absorption behavior, it is inconsistent with the energetic structure evident from the analysis of TTA kinetics. It may nonetheless be instructive to consider in relation to other possible triplet pair states. We propose instead that aggregation alters the vibrational landscape and distorts the $1B_u$ potential energy surface, such that a crossing with the triplet pair state is strongly favored over that with $2A_g$. Full clarification of this intriguing behavior will likely call for both extensive new computational studies of the electronic structure of coupled polyenes and a detailed exploration of vibronic coupling in the aggregates.[54]


DOI: 10.1021/jacs.5b01130
J. Am. Chem. Soc. 2015, 137, 5130–5139

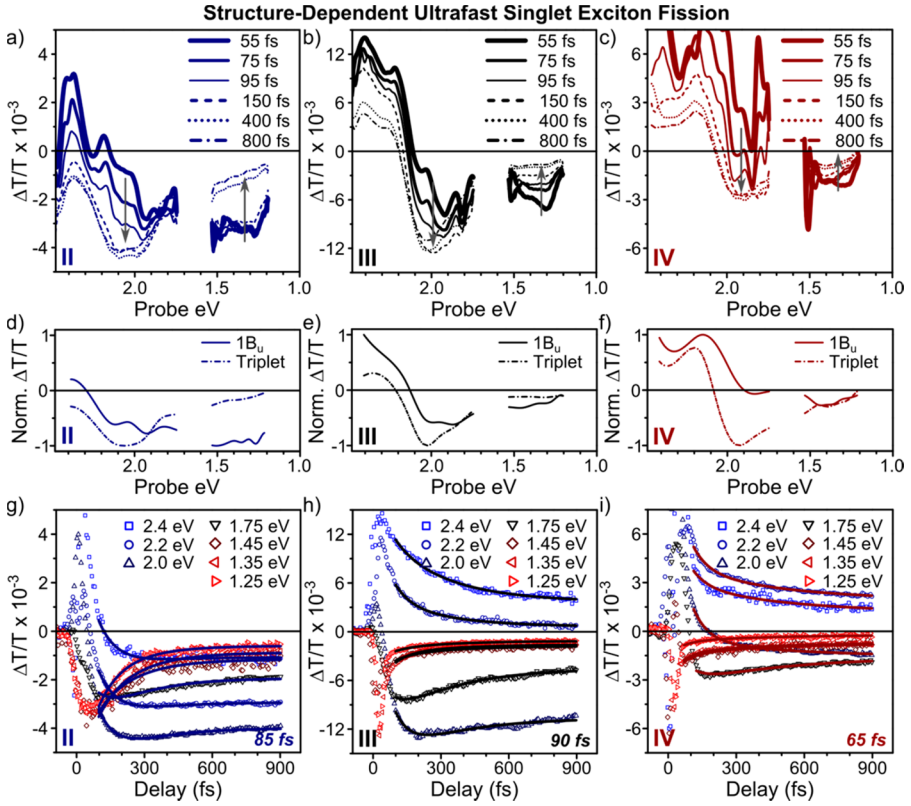


**Figure 7.** Ultrafast triplet formation. (a) Sub-30 fs TA measurements of aggregate II in the visible and NIR spectral regions show a direct transition from the initial singlet (solid) to triplets, already evident by 150 fs. No other states (such as $2A_g$) are observed. Equivalent measurements on aggregates (b) III and (c) IV reveal similar behavior. Arrows indicate the direction of the primary spectral changes. (d–f) Species extracted with a genetic algorithm using a two-state model agree well with the characteristics of $1B_u$ and triplet excitons, and no additional states are needed to describe the data. (g–i) Integrated decay kinetics for each aggregate type (symbols) can all be globally fitted with biexponential functions (lines) capturing the initial singlet fission process and subsequent relaxation of the triplet pair. The singlet fission time constant varies with aggregate structure, from 85 and 90 fs for II and III to 65 fs for IV.

## CONCLUSIONS

We have isolated a system of five distinct aggregates of astaxanthin, allowing adjustment of the intermolecular coupling while maintaining the same monomer chemical and electronic structure. Our transient absorption measurements demonstrated that ultrafast singlet fission occurs in all aggregate types. Sub-ps TA data revealed the presence of only two excitonic states—the bright $1B_u$ singlet exciton and the triplet produced via singlet fission—suggesting a mechanism of singlet fission directly from $1B_u$ rather than via $2A_g$. This model is consistent with our previous high-time-resolution measurements of intramolecular singlet fission in polyenes,[21] and also agrees with the proposal of Wang et al.[25,26] based on studies of zeaxanthin aggregates using a lower time resolution. We confirmed this two-state model with sub-30 fs TA, demonstrating for the first time in a polyene system that intermolecular singlet fission proceeds directly from the initial $1B_u$ state. Furthermore, the purely geminate TTA dynamics immediately following singlet fission indicate that the triplet pair energy is in fact greater than that of $2A_g$, which instead functions merely as an efficient decay pathway back to a vibrationally excited ground state. In other words, the mechanisms of singlet fission and subsequent TTA in polyenes are strikingly similar, whether the fission event is intramolecular like in poly(3-dodecylthienylenevinylene)[21] or intermolecular like in AXT aggregates. These findings raise important questions about the role of low-lying $2A_g$ states. The existence of such a state appears to be a useful sign of the ability to undergo singlet fission, but in polymers and aggregates the state not only does not participate in triplet formation but actually harms the overall yield.

Further theoretical work is required to determine how the triplet pair state forms directly from $1B_u$, a process beyond the scope of current models. Turning to recent high-level calculations of polyene excited states, we note that another triplet pair state, $1B_u^-$, is predicted to lie just below the initial allowed $1B_u$ transition.[55] The coupling between these states would likely be strong, with consequently fast relaxation into the triplet pair. Comparison with the more established polyacenes sheds some light onto the mechanism of singlet fission discussed here. In the most strongly coupled acenes (pentacene and TIPS-pentacene), singlet fission is described as adiabatic, with a rate independent of intermolecular coupling strength. For the majority of the more weakly coupled acenes, however, triplet formation appears to be highly dependent on intermolecular coupling.[15] By contrast, in astaxanthin similar sub-100 fs singlet fission kinetics are observed in strongly (I, V) and weakly (II, III) coupled systems with large (I) and small (V) energetic driving force. This suggests that singlet fission remains in the adiabatic regime in all aggregates and may reflect a unique property of singlet fission in polyenes. This is perhaps not surprising given the widely accepted role of conical intersections in carotenoid photophysics, and it will be important to investigate how vibrational dynamics are implicated in singlet fission within the aggregates. A recent


DOI: 10.1021/jacs.5b01130
J. Am. Chem. Soc. 2015, 137, 5130–5139

study of TIPS-pentacene, for example, has revealed that ultrafast triplet formation is mediated by vibronic coupling between $S_1$ and the triplet pair state,[54] and a similar mechanism may apply here.

Our results also allow important insight into the processes following triplet generation. The observation of two distinct regimes of TTA—fast geminate and slow bimolecular—highlights the unique quantum mechanical properties of triplet pairs generated through singlet fission, which are initially entangled into an overall singlet state. The conversion from geminate to bimolecular recombination reflects a combination of the time scales for triplet pair separation and de-coherence and triplet diffusion, affording a window to study these processes with multipulse techniques or under applied fields and build a model of how and why triplet pairs break apart. More broadly, this system of carotenoid aggregates can serve as a platform to investigate TTA and how it can be controlled through material properties, which is of great interest in the context of triplet-based light-emitting diodes.[56] An understanding of such annihilation processes and their interrelation with intermolecular coupling and triplet generation will be essential to realize the full potential of singlet fission in solar energy harvesting.

## ■ ASSOCIATED CONTENT

### Supporting Information

Circular dichroism, monomer solvatochromism, sensitization TA data, sub-ps TA data for all aggregates and excitation energies, fluence dependence for all aggregates, sub-30 fs TA on aggregates I and V. This material is available free of charge via the Internet at http://pubs.acs.org.

## ■ AUTHOR INFORMATION

### Corresponding Author

*am956@cam.ac.uk

### Notes

The authors declare no competing financial interest.

## ■ ACKNOWLEDGMENTS

This work was supported by the EPSRC (UK) (EP/G060738/1), the European Community (LASERLAB-EUROPE, grant agreement no. 284464, EC's Seventh Framework Programme; and Marie-Curie ITN-SUPERIOR, PITN-GA-2009-238177), and the Winton Programme for the Physics of Sustainability. G.C. acknowledges support by the European Research Council Advanced Grant STRATUS (ERC-2011-AdG No. 291198). J.C. acknowledges support by the Royal Society Dorothy Hodgkin Fellowship and The University of Sheffield's Vice-Chancellor's Fellowship scheme.

## ■ REFERENCES

(1) Smith, M. B.; Michl, J. *Chem. Rev.* **2010**, *110*, 6891−6936.
(2) Smith, M. B.; Michl, J. *Annu. Rev. Phys. Chem.* **2013**, *64*, 361−386.
(3) Wilson, M. W. B.; Rao, A.; Clark, J.; Kumar, R. S. S.; Brida, D.; Cerullo, G.; Friend, R. H. *J. Am. Chem. Soc.* **2011**, *133*, 11830−11833.
(4) Hanna, M. C.; Nozik, A. J. *J. Appl. Phys.* **2006**, *100*, No. 074510.
(5) Jadhav, P. J.; Brown, P. R.; Thompson, N.; Wunsch, B.; Mohanty, A.; Yost, S. R.; Hontz, E.; Van Voorhis, T.; Bawendi, M. G.; Bulović, V.; Baldo, M. A. *Adv. Mater.* **2012**, *24*, 6169−6174.
(6) Ehrler, B.; Wilson, M. W. B.; Rao, A.; Friend, R. H.; Greenham, N. C. *Nano Lett.* **2012**, *12*, 1053−1057.
(7) Ehrler, B.; Walker, B. J.; Böhm, M. L.; Wilson, M. W. B.; Vaynzof, Y.; Friend, R. H.; Greenham, N. C. *Nat. Commun.* **2012**, *3*, No. 1019.
(8) Ehrler, B.; Musselman, K. P.; Böhm, M. L.; Friend, R. H.; Greenham, N. C. *Appl. Phys. Lett.* **2012**, *101*, No. 153507.
(9) Lee, J.; Jadhav, P.; Reusswig, P. D.; Yost, S. R.; Thompson, N. J.; Congreve, D. N.; Hontz, E.; Van Voorhis, T.; Baldo, M. A. *Acc. Chem. Res.* **2013**, *46*, 1300−1311.
(10) Congreve, D. N.; Lee, J.; Thompson, N. J.; Hontz, E.; Yost, S. R.; Reusswig, P. D.; Bahlke, M. E.; Reineke, S.; Van Voorhis, T.; Baldo, M. A. *Science* **2013**, *340*, 334−337.
(11) Tabachnyk, M.; Ehrler, B.; Bayliss, S.; Friend, R. H.; Greenham, N. C. *Appl. Phys. Lett.* **2013**, *103*, No. 153302.
(12) Roberts, S. T.; McAnally, R. E.; Mastron, J. N.; Webber, D. H.; Whited, M. T.; Brutchey, R. L.; Thompson, M. E.; Bradforth, S. E. *J. Am. Chem. Soc.* **2012**, *134*, 6388−6400.
(13) Piland, G. B.; Burdett, J. J.; Kurunthu, D.; Bardeen, C. J. *J. Phys. Chem. C* **2013**, *117*, 1224−1236.
(14) Walker, B. J.; Musser, A. J.; Beljonne, D.; Friend, R. H. *Nat. Chem.* **2013**, *5*, 1019−1024.
(15) Yost, S. R.; Lee, J.; Wilson, M. W. B.; Wu, T.; McMahon, D. P.; Parkhurst, R. R.; Thompson, N. J.; Congreve, D. N.; Rao, A.; Johnson, K.; Sfeir, M. Y.; Bawendi, M. G.; Swager, T. M.; Friend, R. H.; Baldo, M. A.; Van Voorhis, T. *Nat. Chem.* **2014**, *6*, 492−497.
(16) Tavan, P.; Schulten, K. *Phys. Rev. B, Condens. Matter* **1987**, *36*, 4337−4358.
(17) Kraabel, B.; Hulin, D.; Aslangul, C.; Lapersonne-Meyer, C.; Schott, M. *Chem. Phys.* **1998**, *227*, 83−98.
(18) Lanzani, G.; Stagira, S.; Cerullo, G.; De Silvestri, S.; Comoretto, D.; Moggio, I.; Cuniberti, C.; Musso, G.; Dellepiane, G. *Chem. Phys. Lett.* **1999**, *313*, 525−532.
(19) Lanzani, G.; Cerullo, G.; Zavelani-Rossi, M.; De Silvestri, S.; Comoretto, D.; Musso, G.; Dellepiane, G. *Phys. Rev. Lett.* **2001**, *87*, 16−19.
(20) Antognazza, M. R.; Lüer, L.; Polli, D.; Christensen, R. L.; Schrock, R. R.; Lanzani, G.; Cerullo, G. *Chem. Phys.* **2010**, *373*, 115−121.
(21) Musser, A. J.; Al-Hashimi, M.; Maiuri, M.; Brida, D.; Heeney, M.; Cerullo, G.; Friend, R. H.; Clark, J. *J. Am. Chem. Soc.* **2013**, *135*, 12747−12754.
(22) Gradinaru, C. C.; Kennis, J. T. M.; Papagiannakis, E.; van Stokkum, I. H. M.; Cogdell, R. J.; Fleming, G. R.; Niederman, R. A.; van Grondelle, R. *Proc. Natl. Acad. Sci. U.S.A.* **2001**, *98*, 2364−2369.
(23) Papagiannakis, E.; Das, S. K.; Gall, A.; van Stokkum, I. H. M.; Robert, B.; van Grondelle, R.; Frank, H. A.; Kennis, J. T. M. *J. Phys. Chem. B* **2003**, *107*, 5642−5649.
(24) Papagiannakis, E.; van Stokkum, I. H. M.; Vengris, M.; Cogdell, R. J.; van Grondelle, R.; Larsen, D. S. *J. Phys. Chem. B* **2006**, *110*, 5727−5736.
(25) Wang, C.; Tauber, M. J. *J. Am. Chem. Soc.* **2010**, *132*, 13988−13991.
(26) Wang, C.; Angelella, M.; Kuo, C.-H.; Tauber, M. J. *Proc. SPIE* **2012**, *8459*, No. 845905.
(27) Fuciman, M.; Durchan, M.; Šlouf, V.; Keşan, G.; Polívka, T. *Chem. Phys. Lett.* **2013**, *568*−*569*, 21−25.
(28) Horn, D. *Angew. Makromol. Chem.* **1989**, *166*, 139−153.
(29) Auweter, H.; Haberkorn, H.; Heckmann, W.; Horn, D.; Lüddecke, E.; Rieger, J.; Weiss, H. *Angew. Chem., Int. Ed.* **1999**, *38*, 2188−2191.
(30) Manzoni, C.; Polli, D.; Cerullo, G. *Rev. Sci. Instrum.* **2006**, *77*, No. 023103.
(31) Cirmi, G.; Brida, D.; Manzoni, C.; Marangoni, M.; Silvestri, S. De; Cerullo, G. *Opt. Lett.* **2007**, *32*, 2396−2398.
(32) Mori, Y.; Yamano, K.; Hashimoto, H. *Chem. Phys. Lett.* **1996**, *254*, 84−88.
(33) Salares, V. R.; Young, N. M.; Carey, P. R.; Bernstein, H. J. *J. Raman Spectrosc.* **1977**, *6*, 282−288.
(34) Köpsel, C.; Möltgen, H.; Schuch, H.; Auweter, H.; Kleinermanns, K.; Martin, H.-D.; Bettermann, H. *J. Mol. Struct.* **2005**, *750*, 109−115.
(35) Olsina, J.; Durchan, M.; Minofar, B.; Polivka, T.; Mancal, T. *Arxiv* **2012**, *1208*, No. 4958.



DOI: 10.1021/jacs.5b01130
*J. Am. Chem. Soc.* 2015, 137, 5130−5139

(36) Wang, C.; Berg, C. J.; Hsu, C.-C.; Merrill, B. a; Tauber, M. J. *J. Phys. Chem. B* **2012**, *116*, 10617−10630.
(37) Spano, F. C. *J. Am. Chem. Soc.* **2009**, *131*, 4267−4278.
(38) Chábera, P.; Fuciman, M.; Hríbek, P.; Polívka, T. *Phys. Chem. Chem. Phys.* **2009**, *11*, 8795−8803.
(39) Billsten, H. H.; Sundström, V.; Polívka, T. *J. Phys. Chem. A* **2005**, *109*, 1521−1529.
(40) Salares, V. R.; Young, N. M.; Bernstein, H. J.; Carey, P. R. *Biochemistry* **1977**, *16*, 4751−4756.
(41) Bartalucci, G.; Coppin, J.; Fisher, S.; Hall, G.; Helliwell, J. R.; Helliwell, M.; Liaaen-Jensen, S. *Acta Crystallogr. B* **2007**, *63*, 328−337.
(42) Christensson, N.; Zídek, K.; Magdaong, N. C.; Lafountain, A. M.; Frank, H. A.; Zigmantas, D. *J. Phys. Chem. B* **2013**, *117*, 11209−11219.
(43) Bartalucci, G.; Fisher, S.; Helliwell, J. R.; Helliwell, M.; Liaaen-Jensen, S.; Warren, J. E.; Wilkinson, J. *Acta Crystallogr. B* **2009**, *65*, 238−247.
(44) Niedzwiedzki, D. M.; Enriquez, M. M.; Lafountain, A. M.; Frank, H. A. *Chem. Phys.* **2010**, *373*, 80−89.
(45) Albert-Seifried, S.; Friend, R. H. *Appl. Phys. Lett.* **2011**, *98*, No. 223304.
(46) Sliwka, H.-R.; Melø, T.-B.; Foss, B. J.; Abdel-Hafez, S. H.; Partali, V.; Nadolski, G.; Jackson, H.; Lockwood, S. F. *Chem.—Eur. J.* **2007**, *13*, 4458−4466.
(47) Lafferty, J.; Roach, A. C.; Sinclair, R. S.; Truscott, T. G.; Land, E. J. *J. Chem. Soc., Faraday Trans. 1* **1977**, *73*, 416.
(48) El-Agamey, A.; Edge, R.; Navaratnam, S.; Land, E. J.; Truscott, T. G. *Org. Lett.* **2006**, *8*, 4255−4258.
(49) Edge, R.; El-Agamey, A.; Land, E. J.; Navaratnam, S.; George Truscott, T. *Arch. Biochem. Biophys.* **2007**, *458*, 104−110.
(50) Sasaki, Y.; Fujitsuka, M.; Watanabe, A.; Ito, O. *J. Chem. Soc., Faraday Trans.* **1997**, *93*, 4275−4279.
(51) Rademaker, H.; Hoff, A. J.; van Grondelle, R.; Duysens, L. N. M. *Biochim. Biophys. Acta* **1980**, *592*, 240−257.
(52) Gélinas, S.; Paré-Labrosse, O.; Brosseau, C.-N.; Albert-Seifried, S.; McNeill, C. R.; Kirov, K. R.; Howard, I. A.; Leonelli, R.; Friend, R. H.; Silva, C. *J. Phys. Chem. C* **2011**, *115*, 7114−7119.
(53) Liebel, M.; Schnedermann, C.; Kukura, P. *Phys. Rev. Lett.* **2014**, *112*, No. 198302.
(54) Musser, A. J.; Liebel, M.; Schnedermann, C.; Wende, T.; Kehoe, T. B.; Rao, A.; Kukura, P. *Nat. Phys.* **2015**, *11*, 352−357.
(55) Schmidt, M.; Tavan, P. *J. Chem. Phys.* **2012**, *136*, No. 124309.
(56) Wallikewitz, B. H.; Kabra, D.; Gélinas, S.; Friend, R. H. *Phys. Rev. B* **2012**, *85*, No. 045209.



DOI: 10.1021/jacs.5b01130
*J. Am. Chem. Soc.* 2015, 137, 5130−5139